J. Fluid Mech. (2007), *vol.* 588, *pp.* 43–58. © 2007 Cambridge University Press
doi:10.1017/S002211200700763X Printed in the United Kingdom

Eddy structures in a transitional backward-facing step flow

H. P. RANI[1], TONY W. H. SHEU[1] AND ERIC S. F. TSAI[2]

[1]Department of Engineering Science and Ocean Engineering, National Taiwan University, Taipei, Taiwan

[2]Department of Marine Engineering, National Taiwan Ocean University, Taiwan

(Received 11 May 2006 and in revised form 20 May 2007)

In the present study, flow simulation has been carried out in a backward-facing step channel defined by an expansion ratio of 2.02 and a spanwise aspect ratio of 8 to provide the physical insight into the longitudinal and spanwise flow motions and to identify the presence of Taylor–Görtler-like vortices. The Reynolds numbers have been taken as 1000 and 2000, which fall in the category of transitional flow. The present simulated results were validated against the experimental and numerical data and the comparison was found to be satisfactory. The simulated results show that the flow becomes unsteady and exhibits a three-dimensional nature with the Kelvin–Helmholtz instability oscillations and Taylor–Görtler-Like longitudinal vortices. The simulated data were analysed to give an in-depth knowledge of the complex interactions among the floor and roof eddies, and the spiralling spanwise flow motion. Destabilization of the present incompressible flow system, with the amplified Reynolds number due to the Kelvin–Helmholtz and Taylor–Görtler instabilities, is also highlighted. A movie is available with the online version of the paper.

1. Introduction

The phenomenon of flow separation in a backward-facing step channel has received considerable attention owing to its geometric simplicity, physical abundance and its close relevance to some fundamental engineering flows. For instance, this phenomenon often corresponds to drastic losses in the aerodynamic performance of airfoils and in automotive vehicles. Although some of the fundamental flow phenomena have become clear through the two-dimensional solutions, many of the subtleties of third-dimensionality are yet to be learned. As a major benchmark for the two-dimensional numerical simulations, the channel with a backward-facing step has been the subject of experimental (Armaly *et al.* 1983; Nie & Armaly 2004) and numerical investigations (Kaiktsis, Karniadakis & Orszag 1991, 1996; Kim & Moin 1985). Only a few studies are devoted to the three-dimensional aspects of this flow, especially in the steady regime. For example, Armaly *et al.* (1983), Williams & Baker (1997) and Nie & Armaly (2004) focused on the extrinsic sidewall effects both experimentally and numerically. The two-dimensional absolute linear stability of this flow has been examined extensively and was discussed in several publications (Gartling 1990; Gresho *et al.* 1993; Fortin 1997). Barkley, Games & Henderson (2002) revealed, with a linear stability analysis based on numerical simulations, that a steady three-dimensional bifurcation occurs at the critical Reynolds number (based on the step height and the maximum velocity of the upstream profile) of 748. Their computation was performed

on an infinite domain in the spanwise direction and the simulated results suggested their observed instability was of the intrinsic type.

Whereas for transient flows, it is well known that the transitional and turbulent regimes are susceptible to oscillations; in the case of incompressible flows, the oscillations due to the Kelvin–Helmholtz (KH) instability are caused by the interaction between the shear layer and the recirculating flow near the step wall. Due to the KH instability in the shear layer, unsteady vortical structures are generated and convected downstream to produce fluctuations in the velocity and pressure, thus leading to the destabilization of the flow field (Komerath, Ahuja & Chambers 1987; Freitas & Street 1988). In the case of rectangular enclosures, Yao, Cooper & Raghunathan (2004) and Chiang, Hwang & Sheu (1997) showed that this type of three-dimensional destabilized flow exhibits Taylor–Görtler-Like (TGL) longitudinal vortices. Ghia, Osswald & Ghia (1989) computed the two-dimensional backward-facing step flow solutions throughout the laminar regime and found good agreement with the experimental results of Armaly *et al.* (1983). They also postulated that the instability of two-dimensional flow could result from TGL instability after the formation of a secondary separation bubble on the upper wall. This instability leads to a destabilized concave curvature in the main flow. They also proved that the sidewall boundary layer has no contribution to the three-dimensional transition.

Beaudoin *et al.* (2004), in their experimental results for a backward-facing step boundary-layer flow rather than a channel flow, observed five mushroom-like structures near the step wall. They have also carried out the numerical calculations for this problem by considering 'less' complex boundary conditions (for example, no upper wall separation). In their study, the presence of counter-rotating longitudinal vortices was revealed. They observed that this kind of spanwise structure occurs for lower and higher Reynolds numbers. They also showed that the origin of the instability was consistent with the centrifugal instability, and this instability appears in the vicinity of the reattached flow and outside the recirculation bubble.

A perusal of the relevant literature discloses that the presence of TGL vortices is an intrinsic feature of backward-facing step flow. As less attention was generally paid to the presence of TGL vortices, in the backward-facing step flow, the objective of the present study is to investigate the two main instabilities, namely, KH and TGL instabilities in this three-dimensional channel flow. The Reynolds number, Re, in the transitional regime was chosen to depict the flow nature and to show the destabilization of the flow with the value of Re being further increased. The rest of the paper is organized as follows. In § 2, a brief description of the geometry, the initial and boundary conditions is presented. Then the equations governing the fluid motion for the incompressible case are described. Along with the computational procedures, the validation against experimental and numerical data is presented in § 3. In § 4, attention is given to the complex flow evolution, and the interaction mechanism between the primary and secondary eddies. Plausible reasons leading to the formation of TGL vortices are also addressed. Finally, in § 5, a summary of the present study is provided.

2. Computational domain

Figure 1 shows the computational domain and serves to define the geometric parameters for the present work. A step of height $S = 1$ cm was considered, and the corner of the step was taken as the origin of the present coordinate system. Air enters from the inlet channel of height h ($= 0.98$ cm) and flows downstream into the outlet

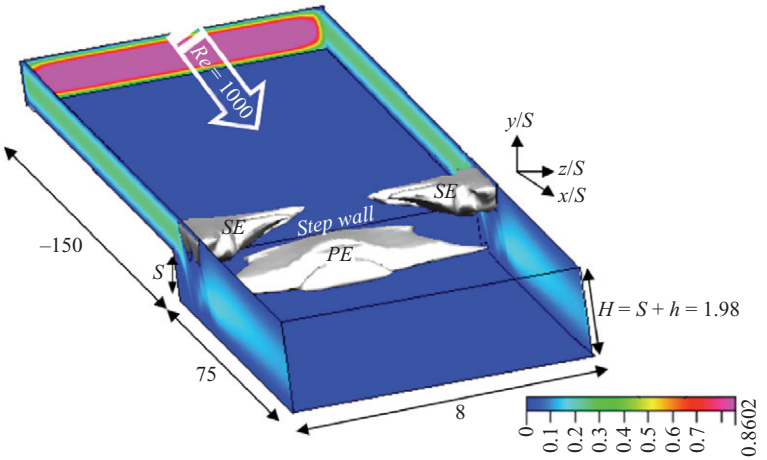

FIGURE 1. Schematic of the backward-facing step flow problem under the current investigation for the case investigated at $Re = 1000$ and time $t = 10$ s. S, PE and SE denote the step wall (= 1 cm), primary eddy or floor eddy and secondary eddy or roof eddy.

channel of height $H(= (1+h))$. The width (W) of the channel was chosen as 8 cm. In this study, an expansion ratio $(ER = \mathrm{H}/(H-S))$ of 2.02 and an upstream aspect ratio $(AR = W/S)$ of 8 were considered. The inflow and outflow lengths $(-150 \leqslant x/S \leqslant 75)$ were considered sufficiently large that the results are independent of these parameters. The fluid contained in this geometry was assumed to have the constant density $(\rho = 1.205\ \mathrm{kg\,m^{-3}})$ and dynamic viscosity $(\mu = 1.81 \times 10^{-5}\ \mathrm{kg\,m^{-1}s^{-1}})$. The flow was assumed to start from rest. The inlet flow at $x/S = -150$ $(1 \leqslant y/S \leqslant 1.98$, for all $z)$ was considered to be hydrodynamically steady and fully developed for the streamwise velocity component (u). The other velocity components (v and w) were set to be equal to zero at the inlet section. The no-slip boundary condition (zero velocity) was prescribed at all wall surfaces and fully developed conditions were imposed at the exit section ($x/S = 75$, for all y and z) for the flow-field variables. The present incompressible fluid motion is governed by the continuity and momentum equations, as shown below.

$$\nabla \cdot \boldsymbol{V} = 0, \tag{1}$$

$$\frac{\partial \boldsymbol{V}}{\partial t} + (\boldsymbol{V} \cdot \nabla)\,\boldsymbol{V} = -\nabla P + \frac{1}{Re}\nabla^2 \overline{V}, \tag{2}$$

where $\boldsymbol{V} = (u, v, w)$, P and t represent the velocity vector, pressure and time, respectively. Hereinafter, the three velocity components u, v and w in the x, y and z directions are referred as the streamwise, transverse and spanwise velocities, respectively. The Reynolds number is given by $Re = \rho u_0 D_h/\mu$, where D_h is given as $2Wh/(W+h)$ and u_0 denotes the average initial velocity. The Reynolds number has the same definition as the one used in the experimental work of Nie & Armaly (2004).

3. Computational details and validation

Numerical simulation of the governing equations subject to the initial and boundary conditions described above was performed by using the commercial computational fluid dynamics software, namely, CFDRC (2003). The mesh was generated in the structured block volumes using the preprocessor CFD-GEOM. The computational

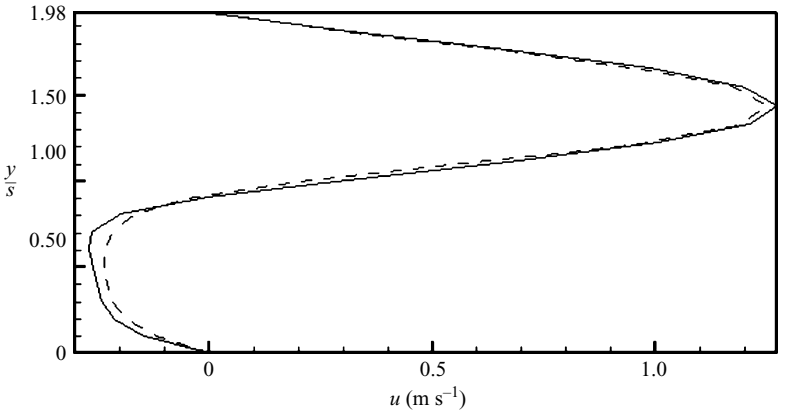

FIGURE 2. The simulated streamwise velocities for $Re = 1000$ at (5, y/S, 4) and $t = 2$ s using two different nodal numbers: —, 113 000; — — —, 89 800.

non-uniform grid distribution was selected to ensure high density near the bounding walls and in the regions near the step wall so as to ensure the accuracy of the simulations. The three-dimensional continuity equation, (1), and transient Navier–Stokes equations, (2), for the investigated incompressible fluid flow were solved numerically using the finite-volume method. The AMG (Algebraic Multi Grid) algorithm was used for the pressure–velocity coupling and the momentum equations are discretized with the third-order upwind scheme. The SIMPLEC scheme has been adopted for the pressure correction. For the unsteady calculations, the implicit backward Euler method was used with a typical time increment as 0.001 s. At the end of each iteration, the residual sum for each of the conserved variables was computed and stored, thus recording the convergence history. The convergence criteria was set so that the scaled residuals must be smaller than 10^{-10} for the mass and the momentum equations. The convergence of a solution was also checked from the mass flow summary. At $Re = 1000$, the flow imbalance was 13 orders of magnitude smaller than the channel flow rate. Hence, this is a well-converged solution.

The transient simulation was terminated at $t = 25$ s to obtain the real time-independent solutions. Figure 2 shows the comparison between the currently employed nodes of 113 000 and approximately 75% of 113 000 nodes using the streamwise velocity. It was observed that when the currently employed nodes are reduced to 25%, then the solutions obtained from these two nodes vary greatly. On a Pentium IV, CPU 2.81 GHz and 2 GB RAM computer, the calculations took 10 days of CPU time using the 113 000 nodes. Since it was difficult to carry out further mesh refinement within the above computer framework, the simulations were carried out using the currently employed 113 000 nodes.

The mass flux was calculated at the outlet to find out whether the upstream channel length ($x/S = 75$) was sufficient for the fully developed flow. As the outlet was drawnout far enough, the mass flux at the outlet was found to be zero. When the downstream length was (x/S) < 75, flow disturbances near the outlet could cause the fluid to come back into the system. This implies that the fully developed flow was not obtained and may give rise to a convergence problem. Hence in the present study, the downstream length was chosen as $x/S = 75$. Detailed descriptions about the CFD code and the solution procedures are found in the CFDRC manual (2003).

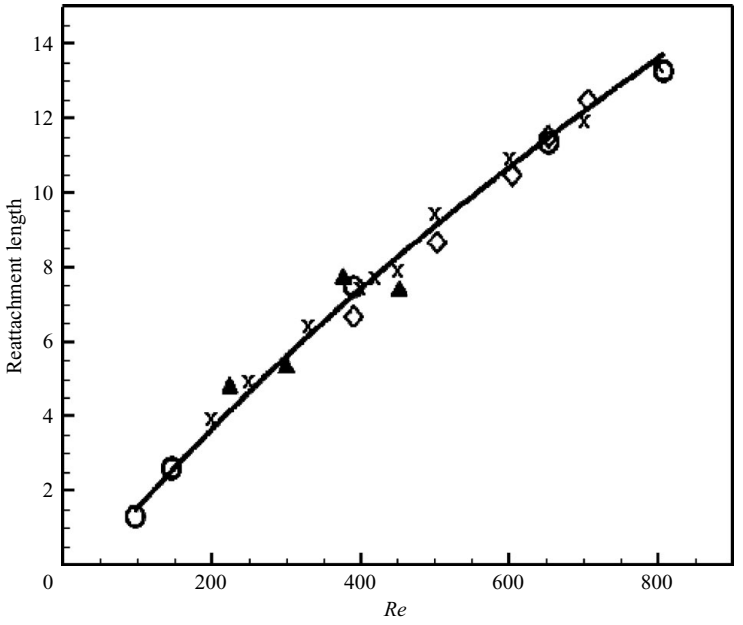

FIGURE 3. Comparison between the simulated and other results in the literature for the primary reattachment length obtained at different *Re*. ———, Armaly *et al.* (1983), ▲, Ku *et al.* (1989); ◇, Jiang *et al.* (1993); ○, Williams & Baker (1997); × present results.

The simulated results were viewed and analysed in the three-dimensional animated plotting tools such as CFD-VIEW and TecPlot.

The present simulated reattachment lengths compared favourably with the numerical simulations by Williams & Baker (1997) and others in figure 3, thus validating the accuracy of the present simulation code. It can be seen from figure 3, the reattachment lengths, which are normalized by the step height, of the primary separation region in the symmetry plane also compare favourably with the results of Ku *et al.* (1989) and Jiang, Hou & Lin (1993) etc. The present three-dimensional results also show excellent agreement with the primary reattachment data of Armaly *et al.* (1983) especially above $Re = 400$, at which the two-dimensional solutions begin to diverge.

4. Results and discussion

The backward-facing step channel flow under the current investigation is laminar and steady for $Re < 738$ and falls in the transitional regime around $Re < 2000$ (Nie & Armaly 2004). At $Re = 1000$, the flow field starts to show the travelling waves that are too mild to excite the formation of TGL vortices. For $Re = 1500$, the flow reveals the existence of the TGL vortices, but shows the symmetric nature. When the Reynolds number is continuously increased to 2000, the periodicity–symmetry-preserving nature disappears and there exist three TGL vortices. Since the main concern of the present study is to analyse the growth of the disturbances due to the TGL vortices, the high *Re*, which will give rise to the complex and transitional flow nature, was not considered. To give a clear picture of the transitional flow structure and the formation of TGL vortices, the two moderate transitional Reynolds numbers, namely, 1000 and 2000, were considered.

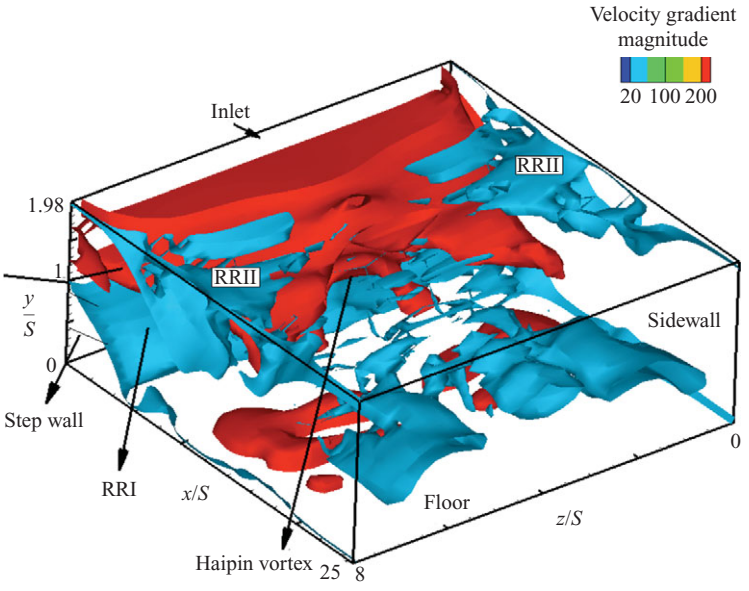

FIGURE 4. Illustration of vortices using the velocity gradient magnitude contours for $Re = 1000$ at $t = 7.8$ s. RRI and RRII denote the recirculation regions.

4.1. *Global flow structure*

Figure 4 shows the global view of the high-velocity gradient shear layer present between the two low-velocity gradient recirculation regions (RRI and RRII) for the case with $Re = 1000$ at $t = 7.8$ s. The inflow near the downstream of the step wall divides the bulk flow into the two recirculation cells. At the interface between these two cells, a shear layer showed its presence (shown in red) and becomes unstable to generate a vertical hairpin-like vortex (Silveira Neto *et al.* 1993; Shih & Ho 1994; Lee, Ahn & Sung 2004). An important feature of this velocity field is the existence of an intense shear layer, where high vorticity is present. The origin of this shear layer is clearly shown in figure 4. In the counter-rotating regime of RRI, each fluid particle rotates towards the floor in the clockwise direction. The RRII region recirculates towards the roof in the anticlockwise direction. At the interface between these two cells, a strong shear layer is prone to instability which leads to a spanwise modulation and results in the roll-up of the individual co-rotating vortices. This instability mechanism was first introduced in the simple case of a linear shear layer by Lord Kelvin and Hermann von Helmholtz at the end of the nineteenth century (see Guyon 2001). Their intention was to explain the wave formation due to the wind stress on the sea surface.

Figure 5 shows the velocity gradient magnitude contours and the instantaneous isosurfaces of the streamwise velocity with the zero magnitude for $Re = 2000$ at $t = 10$ s. The floor and roof eddies, which are present near the step wall, are responsible for the KH and TGL instabilities. In figure 5, the roof eddies are seen to merge together for $Re = 2000$, but are separated for $Re = 1000$ (figure 4). The flow is destabilized owing the presence of roof eddies for increasing Re and this issue will be discussed in § 4.2. At $Re = 2000$, the flow passes between the lower and upper recirculation regions. Because of the stagnant nature of the flow in the regions close to the two endwalls near the downstream of the step wall, there exists a negative

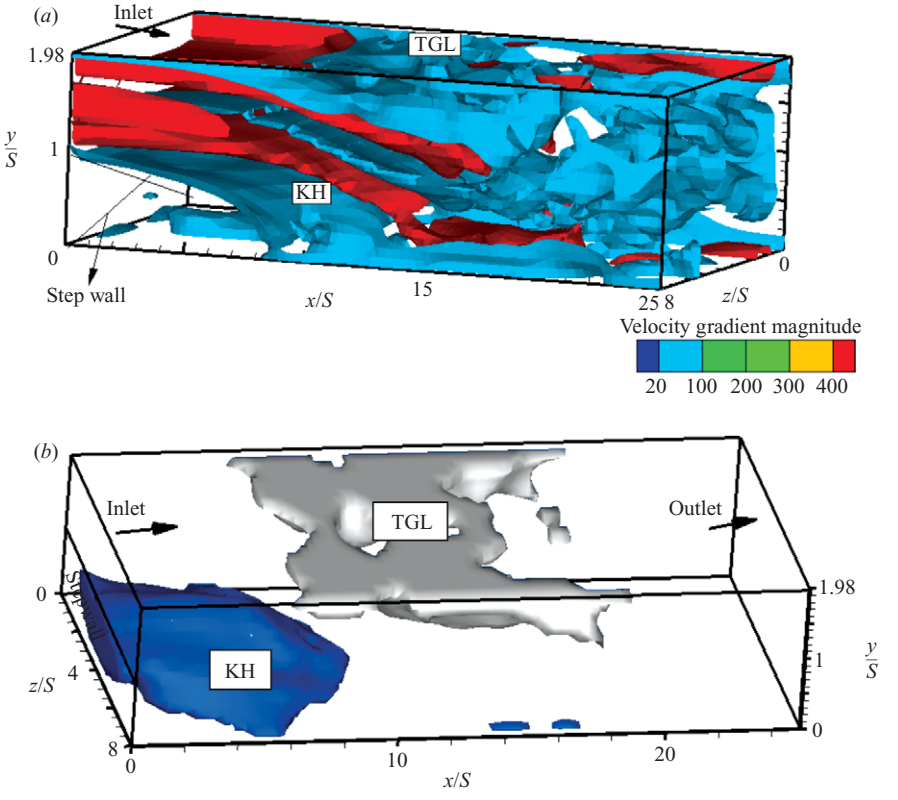

FIGURE 5. Illustration of vortices for $Re = 2000$ at $t = 10$ secs using (a) the velocity gradient magnitude contours and (b) the instantaneous isosurfaces of the streamwise velocity with the zero magnitude. KH and TGL denote the Kelvin–Helmholtz instability and the Taylor–Görtler-like longitudinal vortices, respectively.

pressure gradient which in turn results in a spanwise velocity moving towards the symmetry plane. The streamwise motion, together with an apparent circulation flow pattern at the streamwise plane, constitutes a helical vortex structure. In the present simulation, the primary instability-mechanism from transition to turbulence was found to be a KH instability of the separated shear layer which was triggered by the amplified Re. The KH instability caused the shear layer to roll up. Inside the rolled up shear layer, the entrained disturbances trigger the instabilities. These instabilities lead to a rapid transition to a fully developed turbulent flow. Similar results are observed in the separation bubble for the flow over a flat plate (Wissink & Rodi 2003; Wissink, Michelassi & Rodi 2004).

Figure 6 shows the presence of TGL vortices for the amplified Re. The midplane streamlines for $Re = 1000$ at $t = 10$ s are shown in figure 6(a) and in this figure the wavy nature of streamlines along with KH instability is observed for $Re = 1000$. Comparing figures 6(a) and 6(b), it can be seen that the amplified Re leads to a stronger KH instability, which is located close to the step wall, and is indicated by the increasingly pronounced shear-layer oscillations. From figure 6, vortex pairing and merging in the shear layer could be observed. Also, the lower corner vortex showed its presence. An important difference between figures 6(a) and 6(b) is the occurrence of TGL vortices. In other words, a higher Re is necessary for the occurrence of the TGL

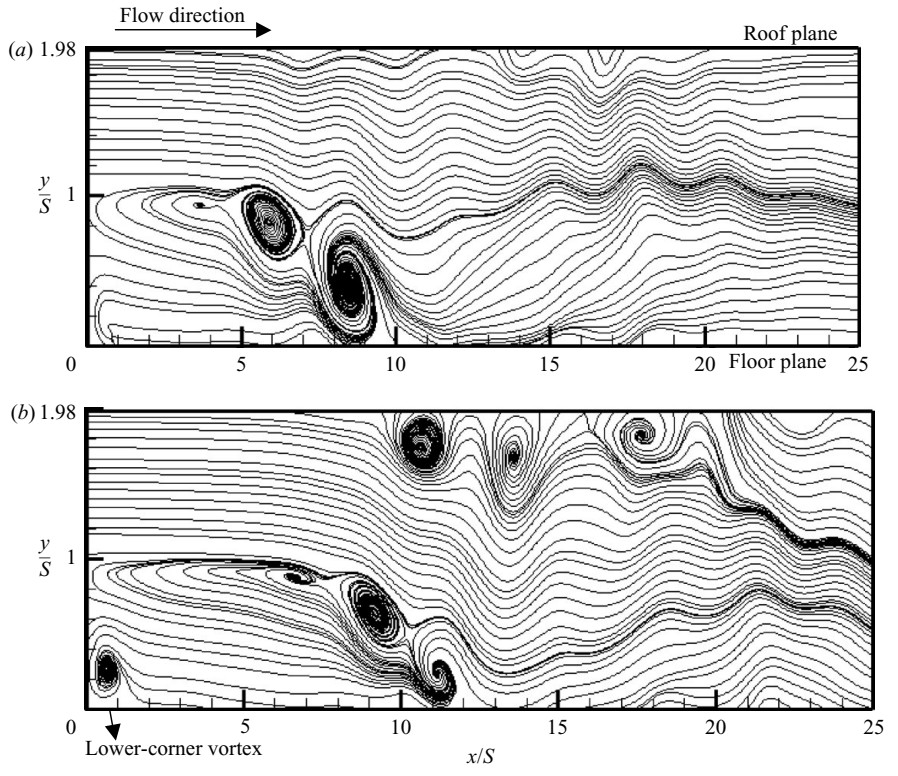

FIGURE 6. The simulated streamlines for (*a*) $Re = 1000$ and (*b*) $Re = 2000$ at $t = 10\,\mathrm{s}$ in the $z/S = 4$ plane.

vortices. For $Re = 2000$, the number of vortices increases from the endwall to the mid plane, which implies that the flow tends to be more unstable in the centreplane. This issue will be discussed in § 4.2.

The instability on the free shear layer is not due to the TGL phenomenon, but rather to the vortex stretching of the KH vortex-structures. The transverse KH vortex core kinks the shear layer waves up and down. The vortex in the recirculation region is stretched to exhibit a lambda-like shape. The vortex-induced velocity field can amplify the instability in the shear layer. Clearly, these shear-layer vortices strongly influence the downstream flow close to the endwalls and the roof, thus possibly dominating the TGL vortex structure. The interaction between these two phenomena (KH and TGL instabilities) accounts for the alternate weakening and strengthening of the vortices.

Previous studies on the backward-facing step flow have been mostly concentrated on the primary eddy/floor eddy close to the step wall. Very few studies have been devoted to the secondary eddy/roof eddy present in the downstream near the step wall. Consequently, in the present study, attention was directed towards the roof eddy. An attempt was made to show that the roof eddy is less stable than the floor eddy.

The streamlines of the particles which are located near the floor eddy and roof eddy are shown in figure 7. The roof and floor eddies are plotted in terms of the zero-velocity isosurface (figure 7*a*). For clarity, the streamlines without the isosurface and the two-dimensional projections of these streamlines are shown in figures 7(*b*) and 7(*c*), respectively, and also in the movie available with the online version of the paper. Once the fluid particles within the roof eddies spiral from the endwall, they

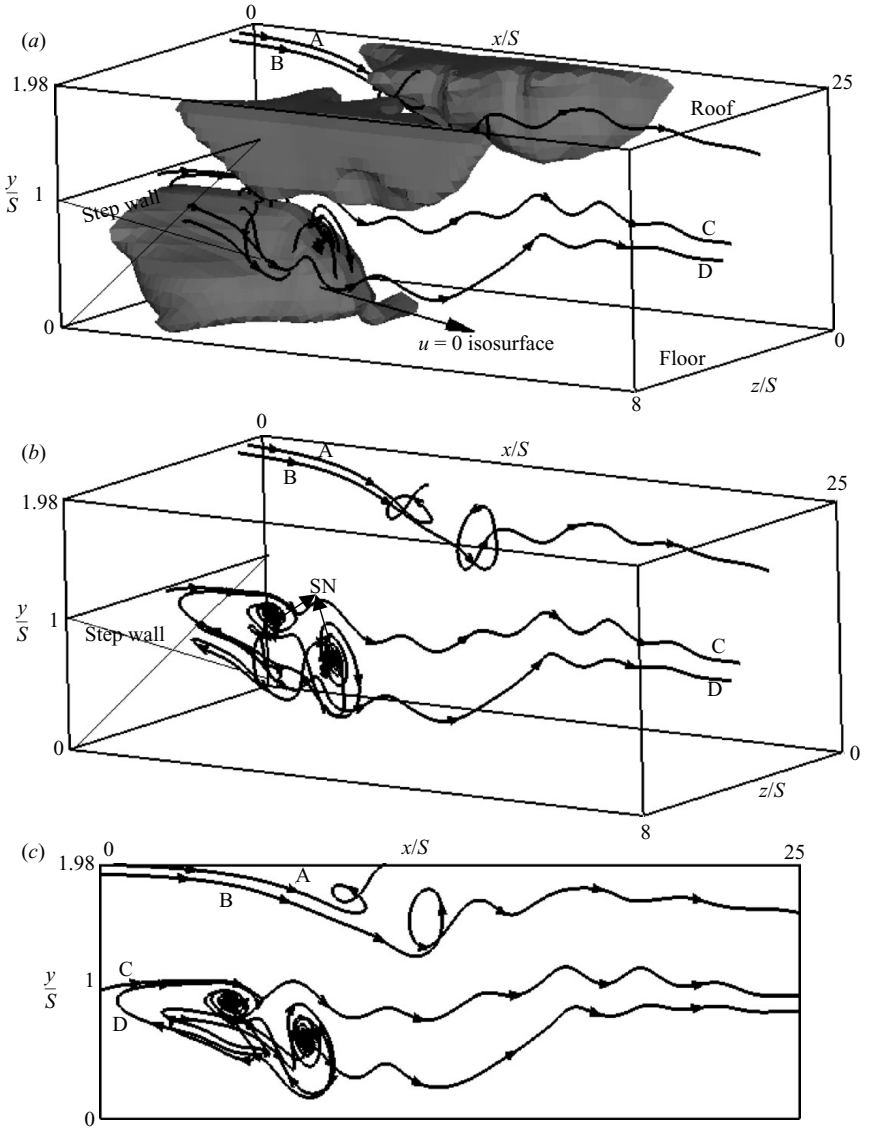

FIGURE 7. Illustration of the spiralling particles at $t = 5$ s for $Re = 1000$. (*a*) Streamlines and $u = 0$ isosurface; (*b*) streamlines; (*c*) two-dimensional view; where SN denotes the spiral node and A, B, C, D denote the particle seeding points at $(x/S, y/S, z/S) = (1, 1.975, 1)$, $(1, 1.9, 1)$, $(0, 1, 4)$ and $(1, 1, 4)$, respectively.

are engulfed into the primary core through the corner vortices. This is followed by a spiralling particle motion, which is characterized by a quick and monotonic migration towards the outlet of the channel. On the other hand, the particles from the floor eddy spiral back-and-forth towards the symmetry plane. In view of the difference in the nature of the spiralling particles, which migrate towards the symmetry plane, it can be clearly seen that the flow in the roof side is more unstable. Another observation is that when the engulfed particle approaches the step wall, there is a higher possibility of this fluid particle being drawn into the primary core of the floor eddy through the attracting spiral node. Figure 7(*c*) (streamline D) confirms this findding. The

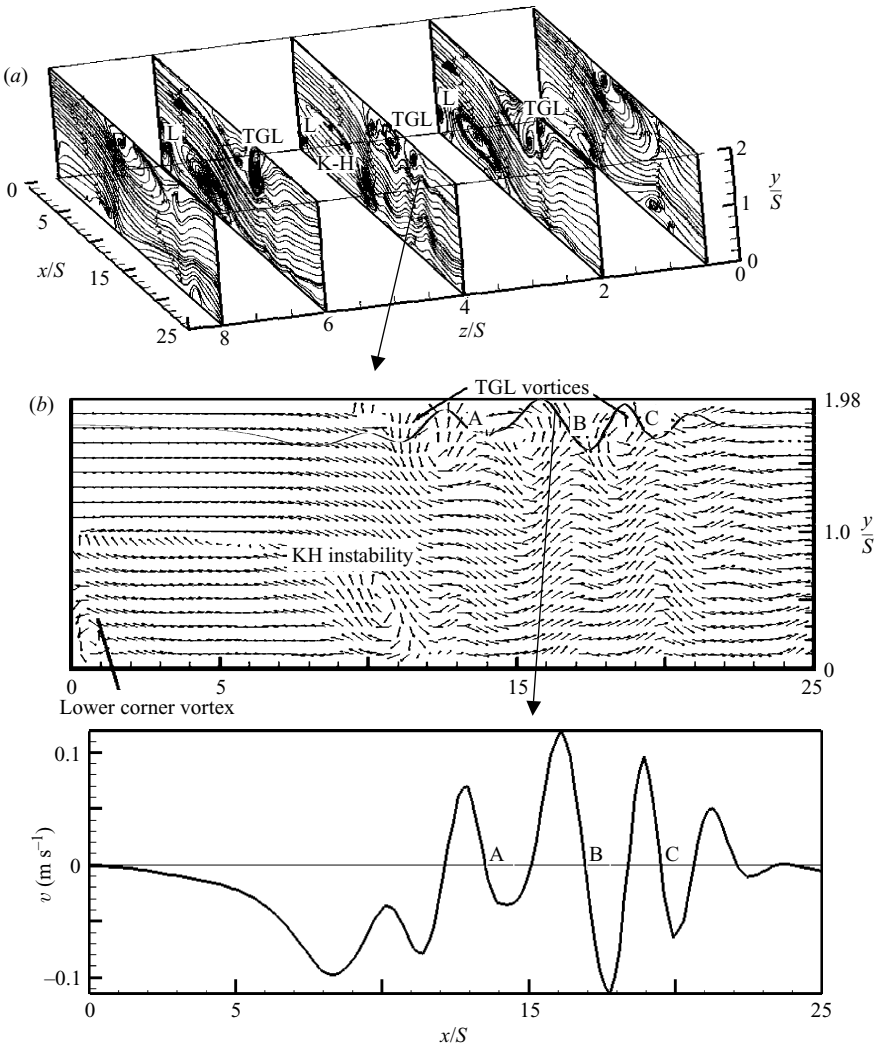

FIGURE 8. (*a*) The simulated streamlines on the (x, y)-planes for $Re = 2000$ at $t = 10$ s. (*b*) The velocity vectors and the transverse $v(x/S,\ y/S = 1.97,\ z/S)$ velocity profile (in solid line), on the centreplane $z/S = 4$. (*c*) The simulated transverse velocity (v) at (x/S, 1.97, 4) along with the zero line. A, B and C denote the locations to identify the TGL vortices. L, TGL and KH denote the lower corner vortex, Taylor–Görtler-like (TGL) longitudinal vortices and the Kelvin–Helmholtz instability, respectively.

back-and-forth spiralling motion of the particle present in the floor eddy aids the flow stability. All the fluid particles that approach the step wall region, $0 \leqslant y/S \leqslant 1$, are entered into the floor eddy. Particles, which are close the roof plane, are drawn upward and, thus, enter into the roof eddy.

4.2. *Taylor-Görtler-like (TGL) vortices*

The crossflow is a typical phenomenon for the three-dimensional flow fields, which could not be simulated accurately in a two-dimensional model. In figure 8, the instantaneous streamlines and vectors at the (x,y)-planes are shown at $t = 10$ s for $Re = 2000$. The strong unsteady phenomena can be observed from this figure. The

transversal vortices in the z-planes show the complex flow nature. In figures 8(a) and 8(b), it can be seen that the TGL vortices exist near the roof plane and the longitudinal vortices exist near the floor plane. The simulated velocity field plotted in the figure has captured some vortex structures occurring within and around the recirculation region, including the lower corner vortex, TGL vortices and the vortices in the free shear layer. These are the typical three-dimensional coherent flow structures. The formation of the longitudinal TGL vortex will contribute to the turbulence generation for the high *Re*. The fluid particles near the step wall region are engulfed into the primary core with the aid of the corner vortex. Corner eddies, as a consequence, aid the spanwise exchange of fluid particles in the channel.

In figure 8(c), the way to identify the TGL vortices for $Re = 2000$ is plotted along the x-direction using the transverse velocity at the location, which is very close to the roof plane. It is observed that the values of transverse velocity fluctuate greatly and have three zero-crossing points (indicated as A, B and C in figures 8b and 8c). A closer inspection of the vector plot shown in figure 8(b) discloses the locations of the TGL vortices, which are identified by the three signs, namely, A, B and C.

The instantaneous streamlines plotted in figure 8 also indicate the presence of KH instability in the shear layer, which is due to the interaction between the external flow and the recirculating flow near the step wall. This instability is promoted by the inflection in the streamwise velocity profile of the shear layer and is particularly strong in the free shear layer. From figure 8, it can also be observed that the backward-facing step flow has inflections, owing to the presence of TGL vortices, but the corresponding instability is weaker. Ghia *et al.* (1989) pointed out that the two-dimensional boundary-layer flows are subjected to locally destabilizing concave curvature of the boundary wall and are known to be susceptible to the classical TGL instability, which could lead to the formation of spanwise-periodic pairs of counter-rotating vortices. Armaly *et al.* (1983) noted that vortex instability is consistent with the onset of the three-dimensionality. They observed that an alternative mechanism leading to the three-dimensional effects is the growth and eventual interaction of the boundary layers on the sidewalls of the experimental apparatus. However, such an effect would tend to diminish with increasing *Re* as the sidewall boundary layers become thinner.

In figure 9, the formation of TGL vortices, in terms of the streamlines and vector plots along with the zero streamwise velocity contour lines, is shown in the $z/S = 2.0$ cutting plane at various time steps. The onset of TGL vortices is mainly due to the increased energy of the disturbances and has been experimentally verified by Aidun, Triantafillopoulos & Benson (1991). At $t = 4$ s, there exist three small vortices near the roof plane and also a free shear-layer vortex. This free shear-layer vortex inherits the property of stable limit cycle, since the inner streamlines spiral outwards while the outer one spirals inwards. At $t = 10$ s, there is a sudden change in the roof and floor eddies. One of the roof eddies disappears and a new corner vortex appears. The fluid particles spiralling towards the endwall tend to be pulled into the primary core by the corner vortex. These engulfed fluid particles spiral quickly and monotonically towards the symmetry plane. This provides a means of destabilizing the flow in the backward-facing step channel. The other two roof eddies change their locations, i.e. one eddy moves towards the floor plane while the other moves towards the roof plane.

Figure 10 shows the roof and floor eddies in terms of the zero contours of streamwise velocity for $Re = 1000$ and 2000 at $t = 10$ s. It can be observed that a developing TGL instability would tend to delay the upper wall separation, thus causing the secondary separation region/roof eddy to occur far downstream. This would in turn decrease

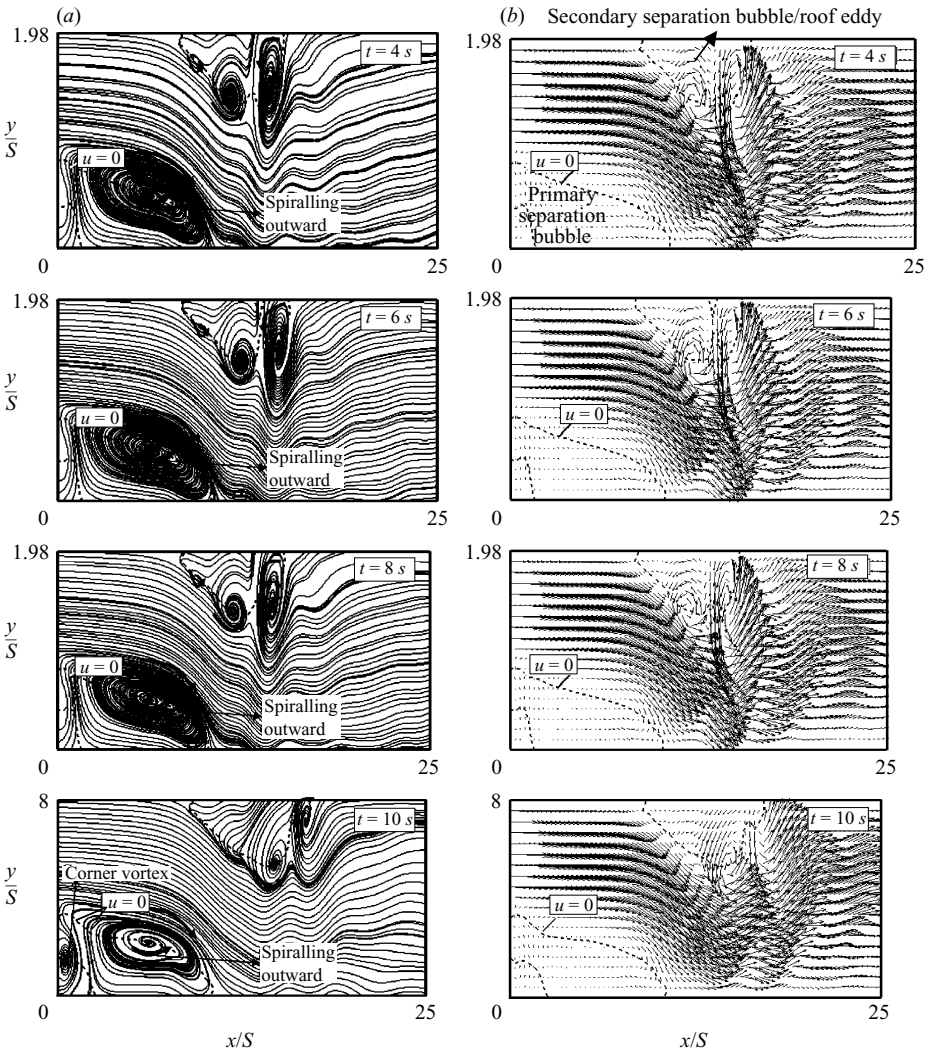

FIGURE 9. The formation of TGL vortices at the $z/S = 2.0$ plane ($4\text{ s} \leqslant t \leqslant 10\text{ s}$) for $Re = 2000$. (*a*) Streamline plots; (*b*) vector plots.

the blockage effect caused by the roof eddy to the main stream and, thus, allows the floor eddy to elongate. In fact, as seen in figure 10, the flow exhibits exactly these characteristics for $Re = 1000$ and 2000.

The values of the streamwise velocity component were examined at (10, 1, 4) and are plotted against time in figure 11(*a*), from which it can be observed that there exist two fundamental modes of fluctuation as shown in figure 11(*b*). In the beginning, the amplitude of fluctuation is 0.115 at frequency of f_1 (= 26) and this is followed by a transitional period. Beyond $t = 8$ s, the periodicity takes another amplitude value, namely, 0.015 at frequency of $f_2 (= 2f_1 = 52)$. These frequencies indicate the presence of frequency-doubling bifurcation. During the transitional period, the flow becomes destabilized (figure 12*b*). Figure 12 shows the comparison of zero streamwise velocity contours near the roof plane at two time intervals for $Re = 1000$ and $Re = 2000$. From figure 12(*a*), it is observed that for $Re = 1000$ the flow is symmetric at $t = 6$ s and

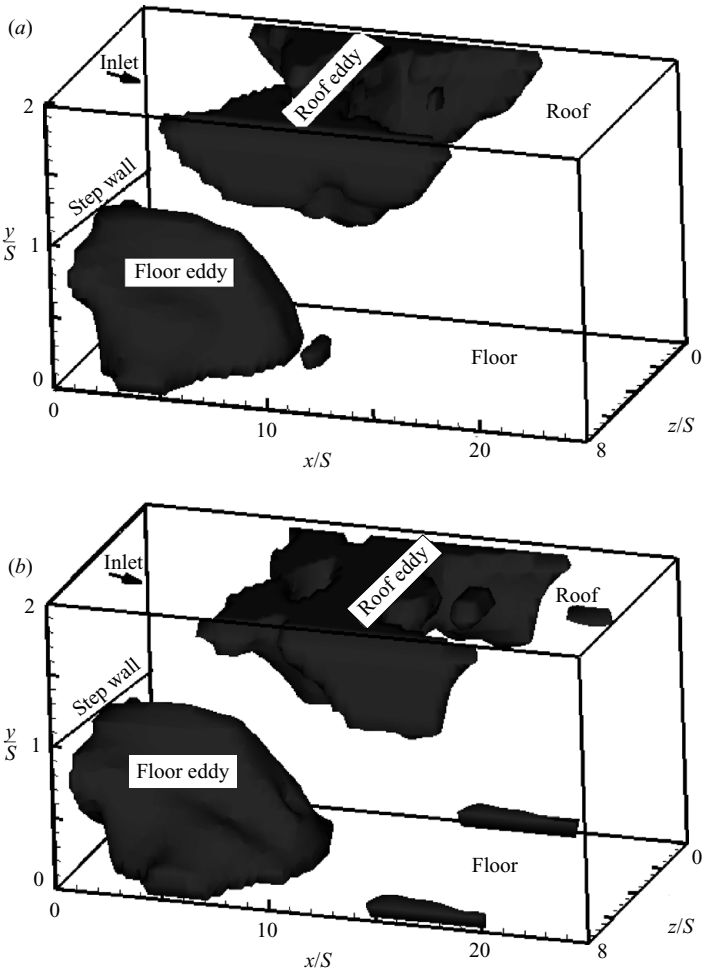

FIGURE 10. The simulated zero-isosurfaces for the streamwise velocity at time $t = 10$ s for (*a*) $Re = 1000$ and (*b*) $Re = 2000$.

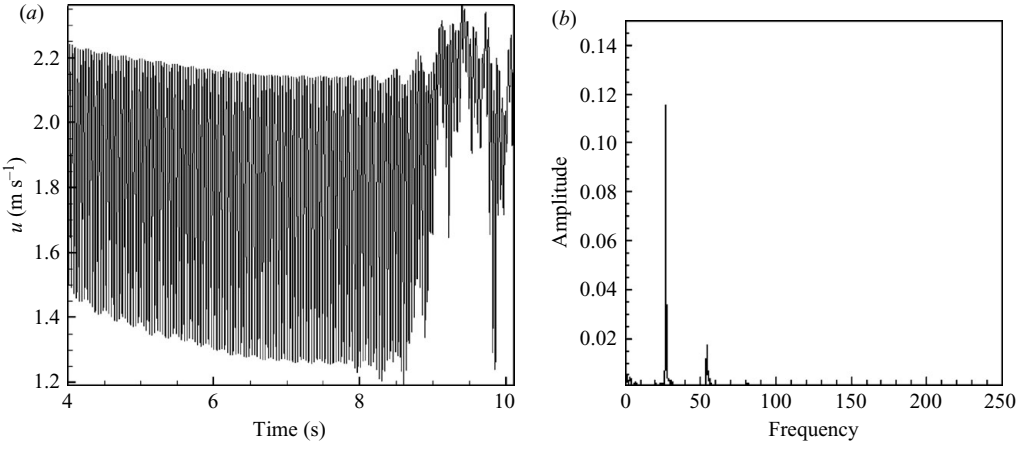

FIGURE 11. The simulated (*a*) time history and (*b*) the corresponding power spectrum of *u*-velocity at the reference point (10, 1, 4) for $Re = 2000$.

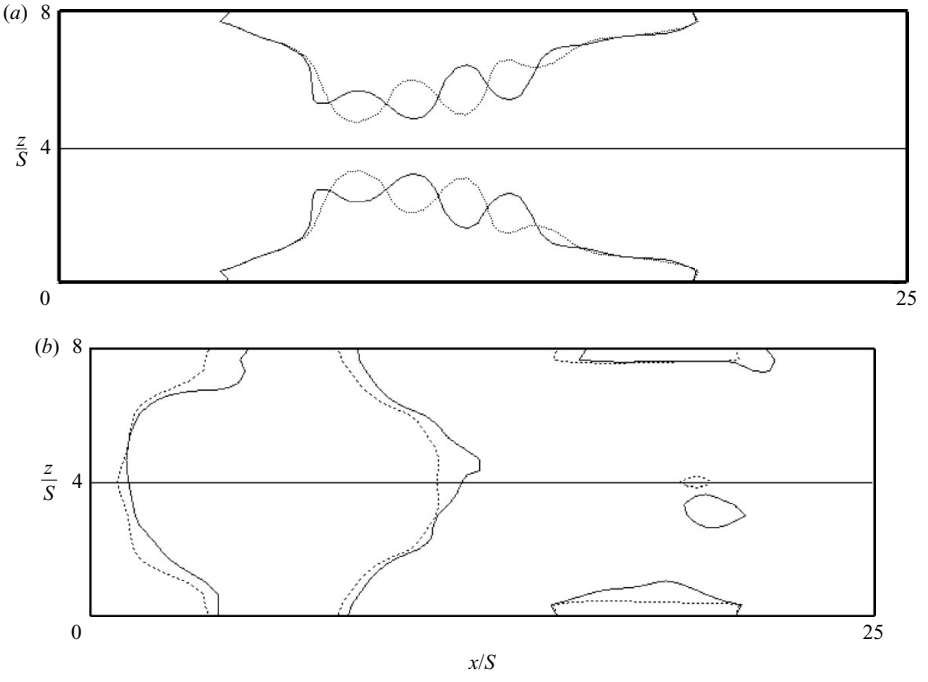

FIGURE 12. The simulated $u = 0$ contour lines at ..., $t = 6$ and ———, 10 s to illustrate the unsymmetric nature at the roof plane ($y/S = 1.975$) for (*a*) $Re = 1000$ and (*b*) for $Re = 2000$.

10 s. Figure 12(*b*) shows that for $Re = 2000$, at $t = 6$ s the flow showed the symmetric nature, whereas at $t = 10$ s the flow lost its symmetry. Thus the increasing values of Re lead to unsymmetric and destabilizing flow.

In summary, the flow is dominated by several interacting features. The high- velocity gradient in the shear layer produced small vortex structures that can cause the KH instability to occur. These vortices are unstable and tend to kink and stretch the flow field, thereby leading to the longitudinal vortices. It is clear that the free shear layer is a complex three-dimensional structure, with both KH instability and TGL vortex interactions. Apart from the TGL vortices and KH instability, for the amplified Re, there exist also a pitchfork bifurcation and a frequency-doubling bifurcation in the flow. The evidence is that the simulated flow structures are not symmetrical about the mid plane ($z/S = 4.0$). As the vortex strength is enhanced and the number of TGL vortices increases in the centre of the downstream flow, the degree of the flow instability increases in the centre region. This flow would become turbulent at some high Re and thus can strongly affect the flow in the region downstream of the channel.

5. Concluding remarks

The geometry of the backward-facing step channel examined in the present study is simple, but the flow physics in this channel is nevertheless rich. The physical complexity arises because of the presence of eddies near the step wall. These eddies possess different sizes and characteristics. Also, the interaction among them is crucial in the laminar instability analysis. In the entire flow evolution, the transport mechanism is rooted largely in the spiralling nature of the flow motion established inside the floor

and roof eddies. Some important findings from the present numerical simulation are given below.

The three-dimensional backward-facing step flow is manifested by the existence of a coiled streamwise velocity component in the downstream owing to the presence of the step wall. Accompanying the streamwise motion, the flow exhibits the dominant recirculation flow pattern. The particles, which are engulfed from the regions near the step wall and the floor plane, spiral monotonically towards the symmetry plane. These particles are the primary source leading to the flow instability because the two flow streams moving in opposite directions tend to collide with each other at the symmetry plane. This instability causes the surface separating the floor/roof eddy to detach from the floor/roof wall. It is this distorted detachment that disrupts the well-balanced force between the centrifugal and pressure-gradient forces, which are present inside the primary recirculating cell. This paves the way for the onset of TGL vortices.

Prior to describing the appearance of TGL vortices, eddies of different sizes and characteristics were studied in detail to understand the complex interaction among the spiralling eddies. In the vicinity of the distorted zero streamwise contour surface, the sign-switching streamwise velocity induces a free shear vortex which is responsible for the KH instability. Also, the flow exhibits the KH instability oscillations in the shear layer and TGL vortices near the roof plane. The strength of the vortices is observed to be large in the centre of the channel downstream. Three TGL vortices are observed in the centre of the channel downstream and only one TGL vortex is seen in the rear endwalls. The simulated strength and number of TGL vortices in the channel downstream imply that the centre of the channel is the origin of flow instability. In the unsteady flow, the flow near the roof plane of the downstream lost its stability as time proceeds. This unstable nature is studied with the help of time-varying plots and isosurfaces.

The flow near the step wall involves several important flow phenomena, including the shear-layer oscillations due to the interaction between the main flow and the recirculating flow. Besides, it is found that a high value of *Re* is required for the occurrence of the KH instability, longitudinal vortices and TGL vortices.

The financial support from National Science Council, under NSC 94-7611-E-002-021 of Republic of China, is gratefully acknowledged.

REFERENCES

Aidun, C. K., Triantafillopoulos, N. G. & Benson, J. D. 1991 Global stability of a lid-driven cavity with throughflow: flow visualization studies. *Phys. Fluids* A **3**, 2081–2091.

Armaly, B. F., Durst, F., Pereira, J. C. F. & Schónung, B. 1983 Experimental and theoretical investigation of backward-facing step flow. *J. Fluid Mech.* **127**, 473–496.

Barkley, D., Gomes, M. G. M. & Henderson, R. D. 2002 Three-dimensional instability in flow over a backward-facing step. *J. Fluid Mech.* **473**, 167–190.

Beaudoin, J. F., Cadot, O., Aider, J. L. & Wesfreid, J. E. 2004 Three-dimensional stationary flow over a backward-facing step. *Eur. J. Mech.* B/*Fluids* **23**, 147–155.

CFDRC, Manual 2003 CFD Research Corporation, 216 Wynn Drive Huntsville, AL 35805, USA. www.cfdrc.com.

Chiang, T. P., Hwang, R. R. & Sheu, W. H. 1997 On end-wall corner vortices in a lid-driven cavity. *Trans. ASMEI: J. Fluids Engng.* **119**, 201–204.

Freitas, C. J. & Street, R. L. 1988 Non-linear transport phenomena in a complex recirculating flow: a numerical investigation. *Intl J. Numer. Meth. Fluids* **8**, 769–802.

Fortin, A., Jardak, M., Gervais, J. J. & Pierre, R. 1997 Localization of Hopf bifurcations in fluid flow problems. *Intl J. Numer. Meth. Fluids*, **24**, 1185–1210.

Gartling, D. K. 1990 A test problem for outflow boundary conditions – flow over a backward-facing step. *Intl. J. Numer. Meth. Fluids* **11**, 953–967.

Ghia, K. N., Osswald, G. A. & Ghia, U. 1989 Analysis of incompressible massively separated viscous flows using unsteady Navier–Stokes equations. *Intl J. Numer. Meth. Fluids* **9**, 1025–1050.

Gresho, P. M., Gartling, D. K., Torczynski, J. R., Cliffe, K. A., Winters, K. H., Garrat, T. J., Spence, A. & Goodrich, J. W. 1993 Is the steady viscous incompressible two-dimensional flow over a backward-facing step at $Re = 800$ stable? *Intl J. Numer. Meth. Fluids* **17**, 501–541.

Guyon, E., Hulin, J. P., Petit, L. & Mitescu, C. D. 2001 *Physical Hydrodynamics*. Oxford University Press.

Jiang, B.-N., Hou, L.-J. & Lin, T.-L. 1993 Least-squares finite element solutions for three-dimensional backward-facing step flow. *NASA TM* 106353.

Kaiktsis, L., Karniadakis, G. E. & Orszag, S. A. 1991 Onset of three-dimensionality, equilibria, and early transition in flow over a backward-facing step. *J. Fluid Mech.* **231**, 501–528

Kaiktsis, L., Karniadakis, G. E. & Orszag, S. A. 1996 Unsteadiness and convective instabilities in two-dimensional flow over a backward-facing step. *J. Fluid Mech.* **321**, 157–187.

Kim, J. & Moin, P. 1985 Application of a fractional-step method to incompressible Navier–Stokes equations. *J. Comput. Phys.* **59**, 308–323.

Komerath, N. M., Ahuja, K. K. & Chambers, F. W. 1987 Prediction and measurement of flows over cavities – a survey. *AIAA Paper* 87-0166.

Ku, H. C., Hirsch, R. S., Taylor, T. D. & Rosenberg, A. P. 1989 A pseudospectral matrix element method for solution of three dimensional incompressible flows and its parallel implementation. *J. Comput. Phys.* **83**, 260–291.

Lee, I., Ahn, S. K. & Sung, H. J. 2004 Three-dimensional coherent structure in a separated and reattaching flow over a backward-facing step. *Exps. Fluids* **36**, 373–383.

Nie, J. H. & Armaly, B. F. 2004 Reverse flow regions in three-dimensional backward-facing step flow. *Intl J. Heat Mass Transfer* **47**, 4713–4720.

Shih, C. & Ho, C. M. 1994 Three-dimensional recirculation flow in a backward facing step. *Trans. ASMEI: J. Fluids Engng* **116**, 228–232.

Silveira Neto, A., Grand, D., Metais, O. & Lesieur, M. 1993 A numerical investigation of the coherent vortices in turbulence behind a backward-facing step. *J. Fluid Mech.* **256**, 1–25.

Williams, P. T. & Baker, A. J. 1997 Numerical simulations of laminar flow over a 3D backward-facing step. *Intl J. Numer. Meth. Fluids* **24**, 1159–1183.

Wissink, J. G. & Rodi, W. 2003 DNS of a laminar separation bubble in the presence of oscillating flow. *Flow, Turbulence Combust.* **71**, 311–331.

Wissink, J. G., Michelassi, V. & Rodi, W. 2004 Heat transfer in a laminar separation bubble affected by oscillating external flow. *Intl J. Heat Fluid Flow* **25** ,729–740.

Yao, H. Cooper, R. K. & Raghunathan, S. 2004 Numerical simulation of incompressible laminar flow over three-dimensional rectangular cavities. *J. Fluids Engng* **126**, 919–927.